Bulletin of Earth Sciences of Thailand

ELASTIC IMPEDANCE INVERSION FOR RESERVOIR AND HYDROCARBON IDENTIFICATION, NORTHERN PATTANI BASIN, GULF OF THAILAND

Monawat Kamolsilp*

Petroleum Geoscience Program, Department of Geology, Faculty of Science,
Chulalongkorn University, Bangkok 10330, Thailand
*Corresponding author email: monawat.k@gmail.com

Abstract

The study area is located in the northern part of the Pattani Basin, Gulf of Thailand. The main reservoirs in this Basin are early to middle Miocene fluvial sandstone. The imaging of these reservoirs using seismic data is always challeng-ing due to the rapid lateral and vertical lithological variations of fluvial systems. Also, the normal faulting in this Basin causes the reservoir to be highly compartmentalized. Rock physics analysis was studied and elastic impedance inversion techniques were applied to improve the reservoir imaging and to predict potential hydrocarbon bearing zone. According to the rock physic analysis, far-angle elastic impedance can differentiate between clean sand and shale in main reservoir interval. P-impedance and near-angle elastic impedance cannot clearly separate sand and shale in the studied intervals. Hydrocarbon sand shows lower values in far-angle elastic impedance compared to the wet sand, whereas P-impedance of hydrocarbon sand and wet sand falls in the same ranges. The far-angle elastic impedance inversion volume was generated. The inversion results show a reasonable match with the blind test wells which conform to the rock physics analysis. The sand mapping reveals that far-angle elastic impedance can detect sand distribution and it can predict potential hydrocarbon zones in the main reservoir interval. The hydrocarbon zones can be further confirmed by using the seismic crossplots of near-angle and far-angle elastic impedance inversion. This study shows that elastic impedance inversion can be used to predict the reservoir distribution and identify potential hydrocarbon zone.

Keywords: Elastic impedance, Inversion, Partial-angle stacked seismic

1. Introduction

The study area lies within the northern part of Pattani Basin, Gulf of Thailand. Reservoir characterization using seismic data is always a challenge in this basin, since the reservoirs in this basin are fluvial sands, which have the rapid lateral and vertical lithological variation. Also, normal faulting in this basin is another factor causing reservoirs to be highly compartmentalized. This results in a high uncertainty of reservoir prediction.

Reservoir characterization using full-angle stack seismic inversion technique was previously studied in the eastern part of the study area by Dangprasitthiporn (2015). The response of full-angle stack seismic data can be predicted by P-impedance parameters. The results show that P-impedance can differentiate lithology in the upper part, whereas it has a limitation to separate the sand and shale in the deeper part. Moreover, P-impedance cannot identify the hydrocarbon-saturated sands. Therefore, P-impedance inverted volume cannot identify the fluid within the reservoir and has limited lithology discrimination in some intervals.

However, the full-angle seismic data often fail to maintain the fluid information and the computed P-impedance has a limitation that it did not integrate the elastic properties such as shear wave velocity and angle of incidence. The elastic properties are involved in the response of seismic data, since the pre-stack seismic data of this area were collected from incidence angle between 5 and 55 degree. This results in inaccurate reservoir characterization using full-stacked seismic inversion technique. Therefore, the study of elastic impedance inversion should be applied with this study area to improve the imaging of reservoir distribution and predic the fluid within the reservoirs.

2. Objectives

The key objectives of this study are to evaluate the rock physics parameters by

integration of elastic properties for hydrocarbon and lithology prediction, and to interpret the elastic impedance inversion volume for mapping reservoir distribution and identifying hydrocarbon bearing zone.

3. Study Area

The study area lies within the northern part of Pattani Basin, Gulf of Thailand. The geological structure is characterized by north-south to northwest-southeast trending of normal faults which show horst-and-graben structures and formed as a result of strike-slip extensional tectonics (Rigo de Righi et al., 2003). The faults in the study area played important roles in the upward migration of hydrocarbons during their active stage and in the trapping of hydrocarbons during their closed stages (Kashi et al., 2005).

The basin fill is mainly non-marine fluvial-deltaic Tertiary sediments which were divided into five stratigraphic sequences by Morley and Racey (2011). Sequence 1 comprises dominantly lacustrine and alluvial syn-rift sediments that deposited during Eocene-Oligocene. The Sequence 2 is mostly fluvial and alluvial plain, post-rift sediments of lower Miocene. The Sequence 3 comprises mainly transgressive fluvial and marginal marine sediments that deposited during early Middle Miocene. The Sequence 4 is an overall regressive fluvial and alluvial deposits of late Middle Miocene. The uppermost, Sequence 5 is predominantly transgressive marginal marine sediments that deposits from the late Miocene to present.

This study focuses mainly on Sequence 2 and 3 which is the main reservoir interval in the study area. The depth of this interval varies from 1100 to 2200 meters and the individual thickness of sandstone reservoir ranges from 2 to 30 meters.

4. Methodology

4.1 Rock Physics

The objective of rock physics analysis is to determine the rock properties that can discriminate lithology and fluid types within reservoirs. Therefore, the seismic volume will be converted into these parameters using the integration with well log data. P-wave velocity (Vp), S-wave velocity (Vs) and density (ρ), P-impedance/ Acoustic Impedance (Z) and elastic impedances (EI) are the rock physics parameters used in this study. Density, P-wave velocity, and S-wave velocity are available in 5 wells, whereas P-impedance and elastic impedance was computed from these parameters.

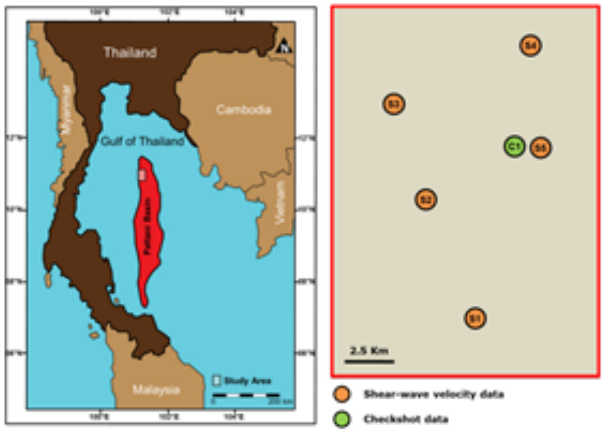

Figure 1 study area is located in the northern part of Pattani Basin. The orange circles show the wells that have S-wave velocity, whereas the green circle shows the well that has checkshot data

Crossplots of P-wave velocity, S-wave velocity, density, P-impedance and elastic impedance were created for different stratigraphic intervals to observe the response of these rock physics parameters for shale volume, gamma ray value, water saturation and porosity. Moreover, the crossplots were analyzed as a function of depth to check the depth dependence of these rock physics parameters.

4.2 Elastic Impedance Inversion

A model-based inversion technique was used to convert the partial-angle stack seismic data into elastic impedance volume. This technique requires the initial low frequency model of elastic impedance which was computed from the well log data. The nature of seismic data is band-limited and the low frequency data are normally missing, whereas well log data contain low to high frequency data.

Therefore, the initial low frequency models of near-angle (14°) and high-angle (28°)

elastic impedance were created using well log data, and this model was used in the inversion process. These initial low frequency models were repeatedly modified by the Generalized Linear Inversion (GLI) algorithm until the synthetic derived from the model matched the seismic data within acceptable limits. The input extracted wavelets are very important to determine the difference between the synthetic derived from the model and the seismic data. The hard constrain was set in this algorithm for comparing the final elastic impedance values to the initial low frequency model values and the output elastic impedance values cannot go beyond these limits (Veeken et al., 2004).

5. Results and Interpretations

5.1 Rock Physics

5.1.1) Crossplots of each parameter versus depth

Figure 2 (a-c) shows the crossplots of density, P-wave velocity and S-wave velocity versus depth color coded by shale volume. The crossplots shows that these 3 main parameters depend on depth and shale volume. The density of sand is lower than shale and shaly sand (labeled by grey square) at all Sequences. The contrast between sand and shale is higher at the shallow part and this contrast decreases with depth. P-wave velocity of sand in Sequence 3 is lower than pure shale and shaly sand respectively. In Sequence 2 and 1, P-wave velocity of sand is similar to the pure shale but it is still lower than the shaly sand. However, some shale in Sequence 1 show very low P-wave velocity compared to sand and other shale especially in the upper part of Sequence 1. S-wave velocity depths. In the upper part of Sequence 3, S-wave velocity of pure shale is similar to sand but in the deeper part (below 1400 meters), pure shale tends to be slower than sand.

Crossplots of P-impedance, near-angle and far-angle elastic impedance versus depth with respect to shale volume are shown in

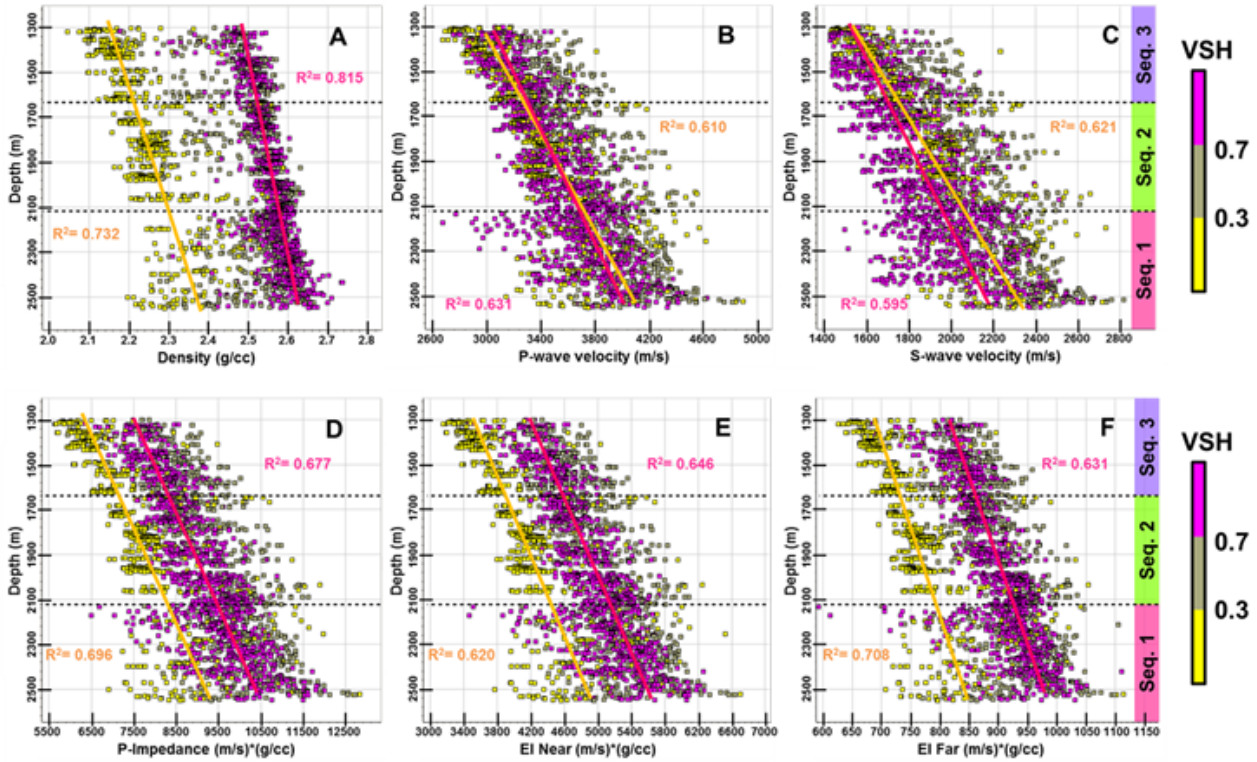

Figure 2 Well log data crossplots of density, P-wave velocity, S-wave velocity, P-impedance, near-angle E-impedance, and far-angle E-impedance versus depth color coded by the shale volume. The black dash lines are the top Sequence 1 and top Sequence 2. The pink lines are fitted with the data point of pure shale (Shale volume > 0.7). The orange lines are fitted with the data point of sand (Shale volume < 0.3). The shaly sands are represented by the grey square (shale volume between 0.3 and 0.7).

Figure 2 (d-e). These three parameters increase with depth following the compactional trend of density and velocity. P-impedance can be used to discriminate sand and shale in Sequence 3 but P-impedance contrast of sand and shale decreases with depth. Therefore, sand and shale can be partially isolated in Sequence 2. In Sequence 1, the low P-impedance shale show overlap with the sand in this section so that P-impedance cannot be used to discriminate the sand and shale in this Sequence. The sand and pure shale show stronger contrast in near-angle and far-angle elastic impedance respectively and the crossplots show that far-angle elastic impedance can be used to discriminate sand and shale in Sequence 2. However, the elastic impedance parameters cannot discriminate sand and shale in Sequence 1 due to the presence of very low velocity shale.

5.1.2) Problem of lithological discrimination in Sequence 1

According to figure 2, P-impedance, near-angle and far-angle cannot be used to isolated sand and shale in Sequence 1, which is different from Sequence 2 and 3. In the well log data (figure 3), this shale shows very high gamma ray values similar to other shale but it has low density, low P-wave velocity, low S-wave velocity and high neutron density compare to other shale. Also, it has P-impedance and Elastic impedance in the same ranges with sand.

Jardine (1997) studied the source rock in Pattani Basin and found that some shale layers in Sequence 1 contain high total organic carbon up to 3%. Narapan (2015) studied the well log response of organic rich sediments in the southern part of Pattani Basin and reveals that some types of organic rich shale show high gamma ray, low density, and high neutron porosity. Also, a rock physics model for characterization of organic-rich shale was studied by Li et al. (2015), and it shows that increasing kerogen content reduces the P-wave velocity, S-wave velocity and density. Therefore, the shale that is present in Sequence 1 with high gamma ray, low density, low P-wave velocity, low S-wave velocity and high neutron density is interpreted as organic rich shale. Therefore, the far-angle elastic impedance cannot be used to isolate sand and shale in Sequence 1 due to the presence of this high organic rich shale.

5.1.3) Lithological discrimination in Sequence 2 and Sequence 3

To observe the response of density, P-wave velocity and S-wave velocity with the shale volume in each Sequence, these 3 parameters were plot against gamma ray and color coded by stratigraphic Sequence (Figure 4a-4c). The gamma ray cut off for sand in Sequence 2 and 3 is below 100 API and this sand has shale volume less than 0.3. The grey shaded area between 100

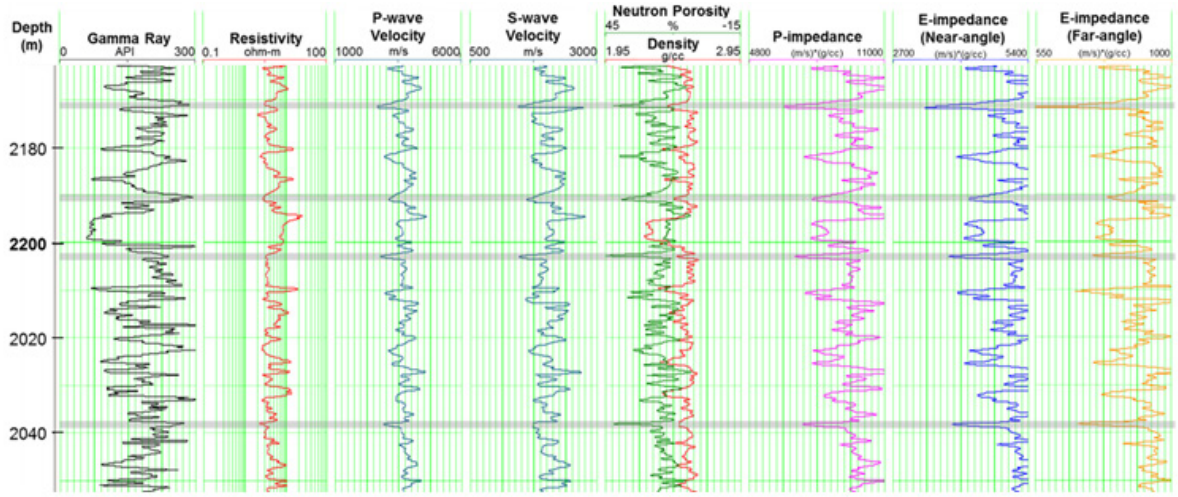

Figure 3 The well log data show high organic rich shale found in Sequence 1 and it is highlighted by the grey shaded area

and 150 API represents the shaly sand which has the shale volume between 0.3 and 0.7. The area above this which has the gamma ray more than 150 API represents pure shale.

The density crossplots show that pure shale in Sequences 2 and 3 have the highest density followed by shaly sand and with the clean sand showing the lowest density value. This plot also shows that density can be used to isolate sand and pure shale in both Sequences. The P-wave and S-wave velocity plotted against gamma ray illustrates that the clean sand has low velocity and when the gamma ray increase, the P-wave and S-wave velocity increase following the increase of shale volume. The velocity increases until the shale volume is around 0.3-0.4 or gamma ray around 100-120 API where above these ranges the velocity begins to decrease when shale volume increase. This observation is similar to the study of Marion (1990) which found that the velocity shows the maximum value at the transition from grain-supported sediment to clay-supported sediments. This effect can be observed in Sequence 2 and 3 where it causes the velocity of sand and pure shale to overlap. Therefore, P-wave and S-wave are hard to be used to discriminate sand and shale in Sequence 2 and 3.

Also, this effect can be observed in the P-impedance plot (Figure 4d) which is computed from P-wave velocity and density. P-wave velocity of sand in Sequence 3 show some slower than pure shale while the P-wave velocity of sand in Sequence 2 show similar value with the pure shale. This causes the higher P-impedance contrast of sand and shale in Sequence 3. This contrast decreases in Sequence 2. Thus, P-impedance of sand in Sequence 2 shows partial overlaps between sand and pure shale. The impedance crossplots (Figure 4e-4f) show that this overlap zone becomes narrower in the near-angle elastic impedance. In the far-angle elastic impedance, this overlap zone disappears and this parameter can be used to define the clear separation trend of sand and shale in Sequence 2. When

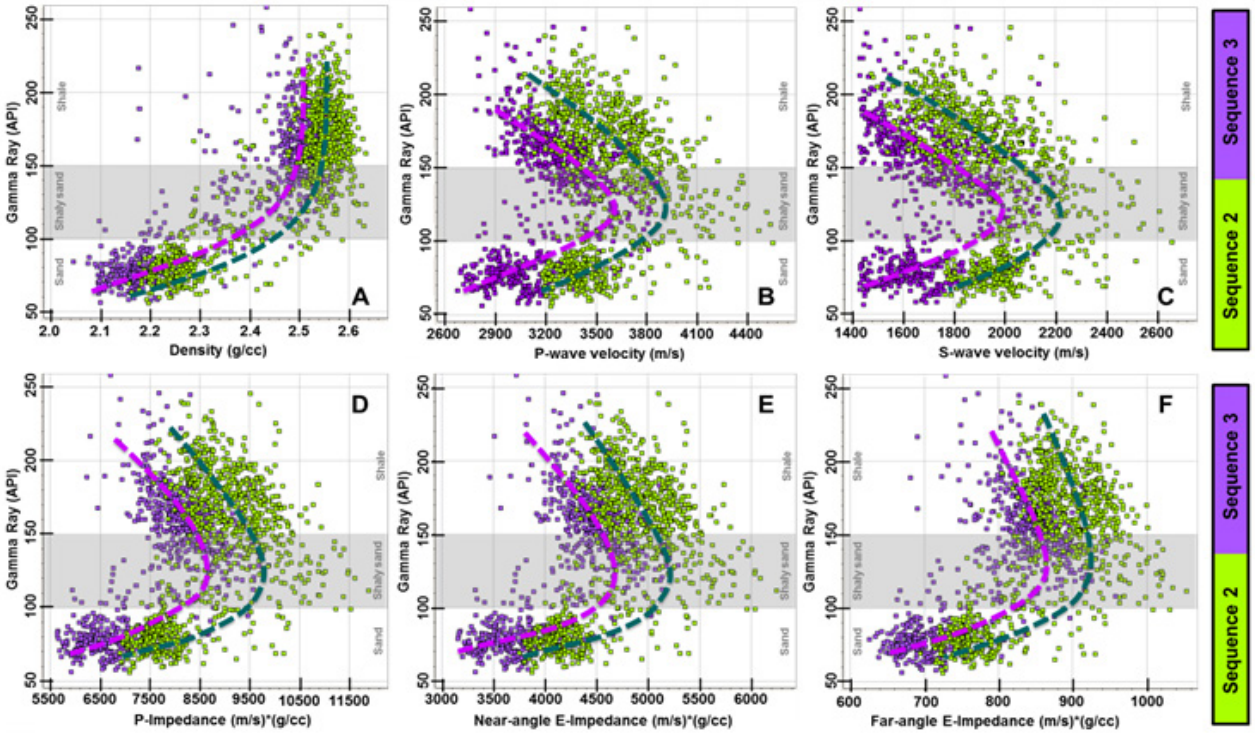

Figure 4 Well log data crossplots of density, P-wave velocity, S-wave velocity, P-impedance, near-angle E-impedance, and far-angle E-impedance versus gamma ray with respect to stratigraphic Sequences 2 and 3. The light green dashed lines are fitted with the data point in sequence 2 while, the purple dashed lines are fitted with the data point in sequence 3. The shapes of the line in figures 4a-4b show that density is the dominant parameter for sand and shale discrimination, while figures 5d-5e show the increasing of dominant density in the higher-angle E- impedance.

comparing the three crossplots of P-impedance, near-angle and far-angle elastic impedance versus gamma ray, the P-impedance plot shows similar trend of P-wave velocity crossplot which the shaly sand shows the higher distinctive values compared to the shale. In near-angle and far-angle the trends change to be more similar with the density plot in which the higher angle elastic impedance. the impedance of shale is shifted to fall in the same ranges with shaly sand. This implies the increasing effect of density in the higher angle of computed elastic impedance. This results in a better discrimination between sand and shale in the higher angle elastic impedance.

Therefore, elastic impedance inversion in Sequence 2 and 3 from far-angle stack data is expected to provide better sand to shale contrast resulting in a clearer imaging of geological channel-like features than near-angle stack data and full stack data.

5.1.4) Hydrocarbon Discrimination

Crossplots (figure 5) of P-impedance and elastic impedance versus GR were color coded by water saturation in order to identify the relationship of these parameters with the water saturation. P-impedance plot in Sequence 2 and 3 shows that hydrocarbon sand and wet sand has the same impedance ranges, whereas in elastic impedance the hydrocarbon sand has a lower impedance value compared to the wet sand. In far-angle elastic impedance, the hydrocarbon sand shows increasingly lower values than wet sand when compared with near-angle elastic impedance. This observation is caused by an AVO effect that makes the low water saturation sand to be emphasized in the higher angle elastic impedance. The rough cut off for hydrocarbon sand in Sequence 2 is 660 (m/s)*(g/cc), whereas the cut off for hydrocarbon sand in Sequence 3 is 730 (m/s)*(g/cc). Although, this

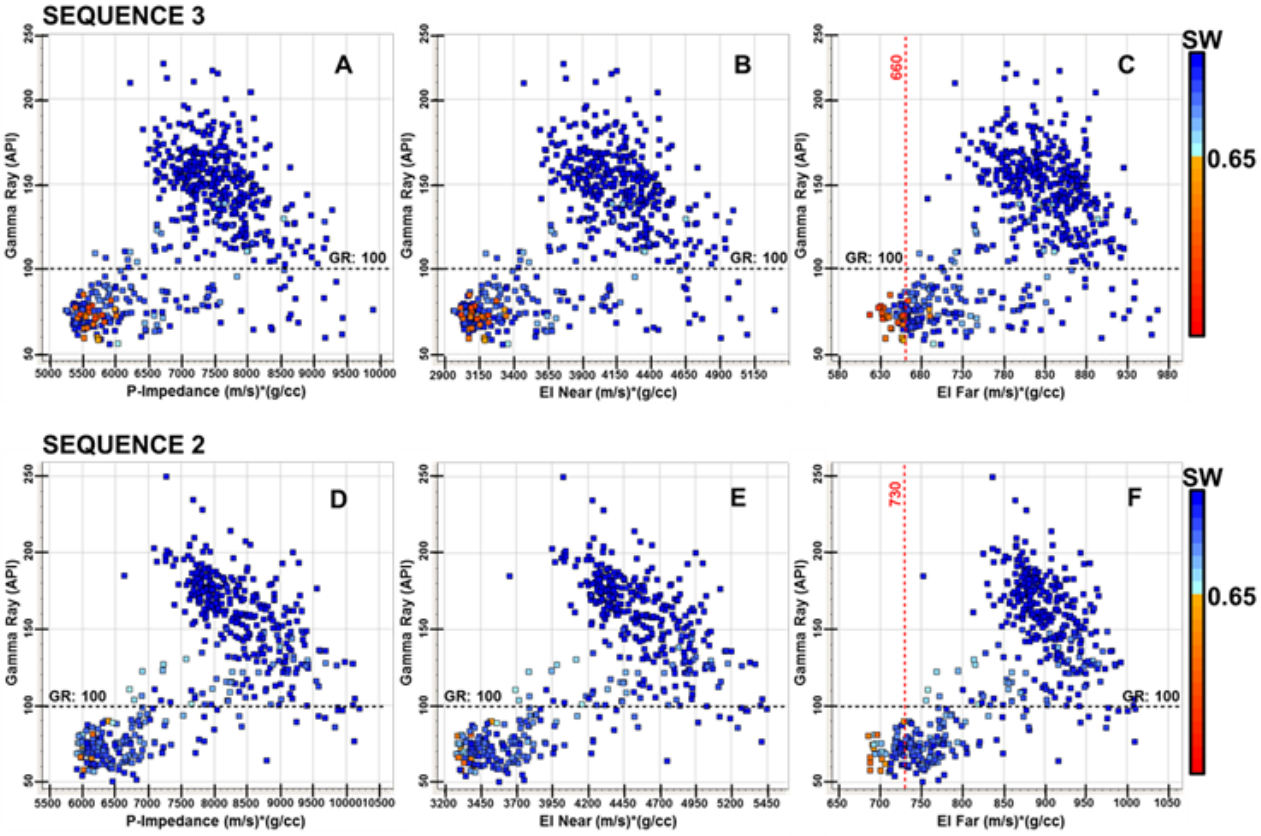

Figure 5 Well log data crossplots of P-impedance, near-angle E-impedance, and far-angle E-impedance versus gamma ray with respect to water saturation for sequence 2 and 3. The black dash lines are the gamma ray cut off for sand. The red

hydrocarbon sand was emphasized in the far-angle elastic impedance some overlap between wet sand and hydrocarbon sand are present. Many previous crossplots show that far-angle elastic impedance is related with many parameters such as depth, shale volume, and porosity. Therefore, the high porous clean wet sand or wet sand located at shallow depths in this area may show low values of far-angle elastic impedance like low water saturation sand resulting in some overlap zones.

Based on results of crossplot analysis, the far angle elastic impedance can be used to discriminate sand and shale in Sequence 2 and 3. Also it can indicate the high porous sand zone and emphasize the possible hydrocarbon in the study area. Therefore, far-angle elastic impedance inversion technique is suitable with Sequence 2 and 3 in this study area. This technique can provide the far-angle elastic impedance volume which can be used to predict the possible reservoir target from the seismic data. In Sequence 1, there is a limitation for lithology discrimination due to the presence of high organic rich shale and low density contrast between sand and shale. Moreover, sand character in Sequence 1, which is located deeper than Sequences 2 and 3, commonly has very thin beds (less than10 meters). These sands are hard to be observed in the seismic data because they are below the seismic resolution. Thus, the inversion technique will be focused only on Sequence 2 and 3 in the study area.

5.2 Elastic Impedance Inversion

5.2.1) Initial Low Frequency Model

Low frequency data normally are missing from the seismic data. Therefore, the model was built by filtering the elastic impedance log data by high pass filter. The computed elastic impedance logs at 14° and 28° from 5 wells were used to build the initial low frequency model for the near-angle and far-angle stack seismic volumes respectively. Each elastic impedance log was interpolated along the interpreted horizons which are top Sequence 1, top Sequence 2 and top Sequence 3. The models were created using this data set. These models show the increasing elastic impedance values with depth caused partly by the compaction process.

5.2.2) Elastic Impedance Inversion

The near-angle and far-angle stack seismic volume were inverted to the elastic impedance volume using the model based inversion technique. The hard constraint option was selected in the inversion process to control the inverted elastic impedance result to be aligned with the low frequency model. The average block size of inverted volume depended on the sampling rate of seismic data which was set to be 4 milliseconds.

The inverted elastic impedance logs created from the integration of seismic data along wellbore with low frequency model were compared to the original elastic impedance log. The result shows the high correlation values for both near-angle and far-angle inverted data at 0.86 and 0.81 respectively and this indicates appropriate parameters using in the inversion process.

5.2.3) Comparison of Elastic Impedance Inversion Volume with Blind Test Wells

The comparison of the well log data and inverted elastic impedance volume was performed with the wells which were not use in the inversion process. The elastic impedance volume in near angle and far angle shows the conformable results with this blind test well in both Sequence 2 and Sequence 3.

Figure 6a shows the results of near-angle elastic impedance volume with blind test well between Sequence 2 and Sequence 3. The well log curves shown in this figure are gamma ray log (black) and resistivity log (blue). The low near-angle elastic impedance corresponds to the low gamma ray log of the blind test well. The near-angle elastic impedance of sand ranges from 3100 to 4000 (m/s)*(g/cc) which is represented by the yellow to light green colors. Also, the results of far-angle elastic impedance volume with blind test well between Sequence 2 and Sequence 3 are shown in the figure 6b. The low far-angle elastic impedance aligns with

Tthe low gamma ray log of the blind test well. The far-angle elastic impedance of sand ranges from 620 to 750 (m/s)*(g/cc) which is represented by the yellow to green colors.circles in figure 6). These hydrocarbon bearing sands have elastic impedance less than 650 (m/s)*(g/cc). This agrees with the results of the crossplots analysis from well log data.

5.2.4) Seismic and Well-log Crossplot Analysis

Typically the difference in near-angle and far-angle inversion results should be considered in locating the potential hydrocarbon bearing zone. The well log crossplots of near-angle and far-angle elastic impedance reveals the potential hydrocarbon zone that deviated from the wet sand trend in the plot (figure 7a).

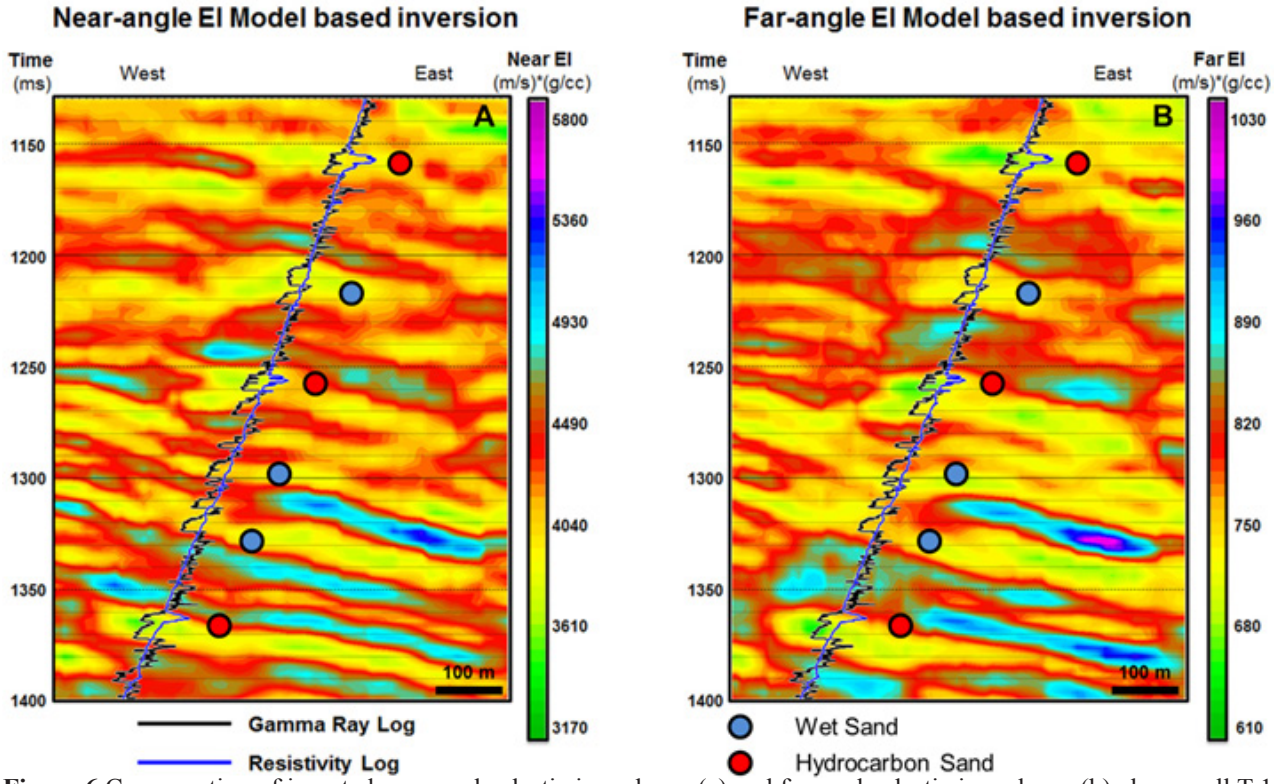

Figure 6 Cross-section of inverted near-angle elastic impedance (a) and far-angle elastic impedance (b) along well T-1 within Sequence 2 and 3. Gamma Ray (Black) and Resistivity (Blue) are displayed to show the result of blind test well.

When compare the two inverted volumes, sand and shale c an be discriminated better in the far-angle elastic impedance volume because some shale interval in near-angle elastic impedance volume shows similar response with the sand. Moreover, the hydrocarbon sands and wet sands in the near-angle elastic impedance volume fall in the same ranges, whereas the hydrocarbon sands in far-angle elastic impedance have lower values than the wet sand (red circles in figure 6). These hydrocarbon bearing sands have elastic impedance less than 650 (m/s)*(g/cc). This agrees with the results of the crossplots analysis from well log data.

The hydrocarbon zone was identified in the plots. This zone in the well log crossplot was applied to the seismic crossplot of near-angle versus far-angle elastic impedance inversion (figure 7b) to define the potential hydrocarbon area in the elastic impedance inversion volume.

The potential hydrocarbon zone in the inversion volume detected by this method is conformable with the result of the well log data of blind test wells. Figure 7c shows the cross section of elastic impedance inversion volume and the potential hydrocarbon zone identified by the crossplots method which is highlighted by the red color and it shows a good agreement with the result of well log data in both Sequence 2 and 3.

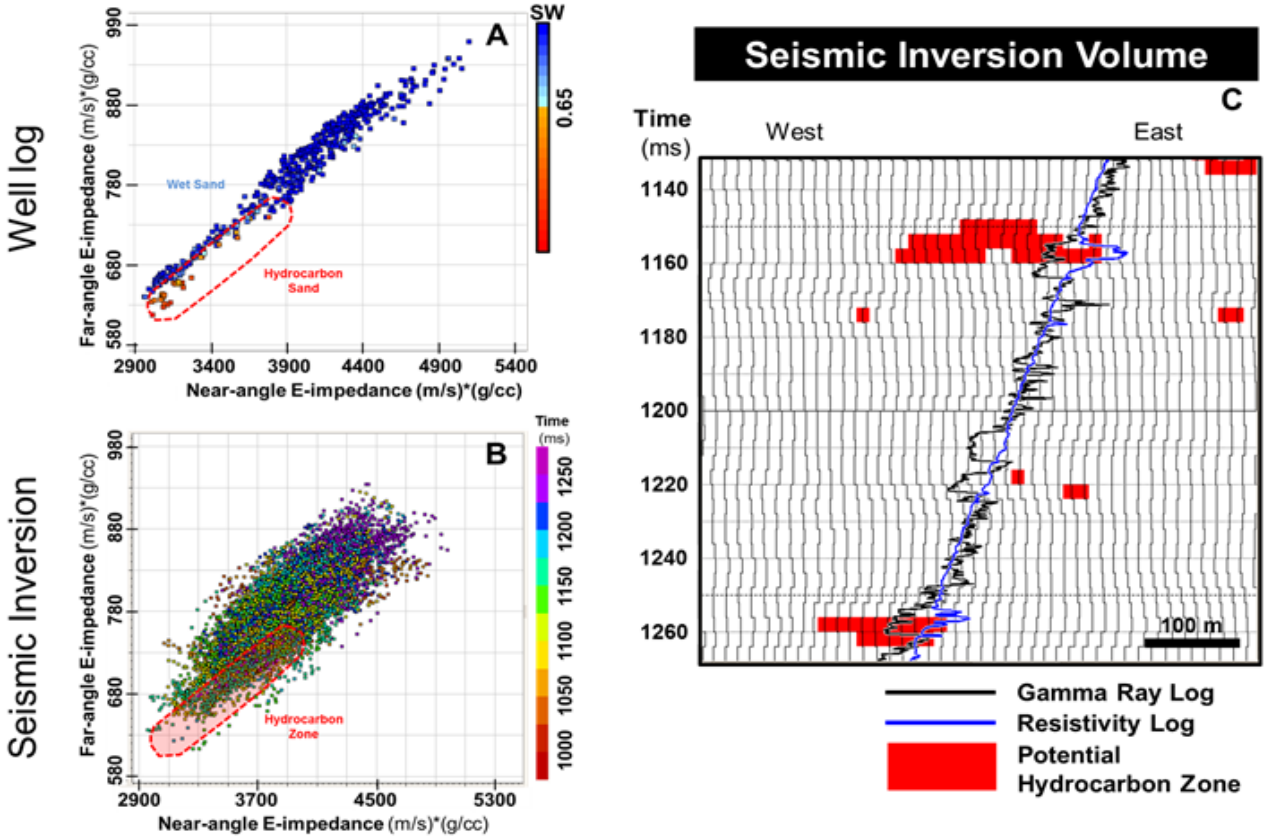

Figure 7 The well log crossplots between inverted E-impedance of near-angle and far-angle color coded by time (millisecond) and the hydrocarbon zones were selected based on the results of well log data (A). This zone in the well log crossplot was applied to the seismic crossplot (B). The potential hydrocarbon zone predicted by seismic crossplots is highlighted by the red color and it shows conformable results with the blind test wells (C)

5.2.5) Sand Mapping in the Far-angle Elastic Impedance Volume

The horizon slices within the far-angle elastic impedance inversion volume indicate the geological channel-like feature found in Sequence 2 and Sequence 3. The overall results align with the crossplot analysis of well log data. Figure 8a show the sand distribution in Sequence 3, whereas figure 8b shows the sand distribution in Sequence 2. According to the rock physics crossplots and the observation in inverted volume, sand body is represented by the elastic impedance lower than 750 (m/s)*(g/cc) for Sequence 3 and 820 (m/s)*(g/cc) for Sequence 2. This zone is represented by yellow, red and white colors.

The circles shown in the map represent the proved results of blind-test wells from well log data. According to these four sand trend maps, there are 14 wells in sequence 3 and 8 wells in sequence 2, which penetrated the yellow to red zones and are associated with the geological channel-like features. The results show that all of them penetrated the sand in that interval.

Furthermore, the hydrocarbon sands are mostly represented by the zone highlighted by grey to white colors and have far-angle elastic impedance values less than 650 (m/s)*(g/cc) for Sequence 3 and 730 (m/s)*(g/cc) for Sequence 2. The identification of these zones as hydrocarbon bearing is further confirmed by these anomalies being located against the fault and aligned with the structure map. This condition has been proven by 8 wells. When we focus on the technique that uses the crossplot of near-angle and far-angle inverted volume to identify the potential hydrocarbon zone, hydrocarbon sand in 5 wells from 8 wells can be detected by this technique. for Sequence 3 and 730 (m/s)*(g/cc) for Sequence 2. The identification of these zones as hydrocarbon

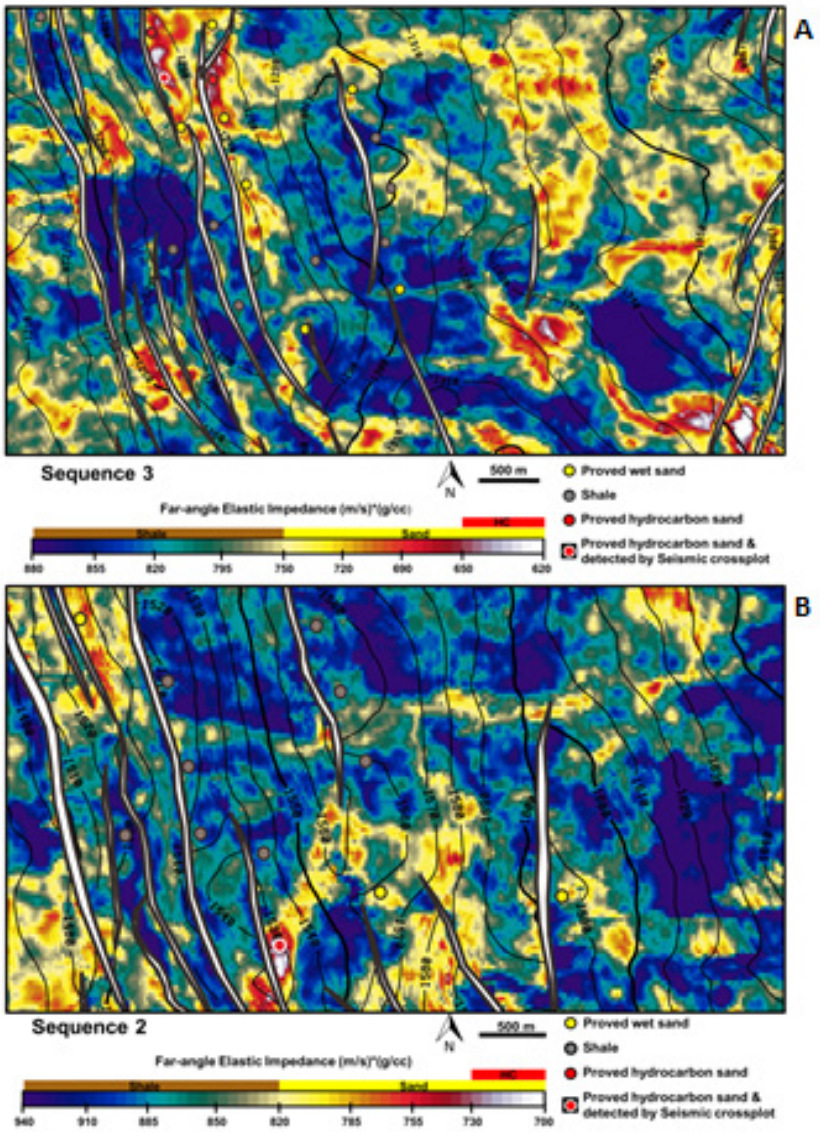

Figure 8 The horizontal slice within far-angle elastic impedance inversion volume is over-layed by two-way-time structural contour map. It shows possible reservoir distribution in Sequence 2 and 3. The circles show the result of well log data from blind-test wells.

bearing is further confirmed by these anomalies being located against the fault and aligned with the structure map. This condition has been proven by 8 wells. When we focus on the technique that uses the crossplot of near-angle and far-angle inverted volume to identify the potential hydrocarbon zone, hydrocarbon sand in 5 wells from 8 wells can be detected by this technique.

6. Conclusion

Rock physics analysis was studied and elastic impedance inversion techniques were applied to the data set in the northern part of Pattani Basin, Gulf of Thailand. The conclusions are summarized below;

Sand and shale have low P-impedance contrast in Sequence 2 due to lower contrast of density and P-wave velocity but far-angle elastic impedance can clearly differentiate sand and shale in both Sequence 3 and 2. However, P-impedance and far-angle elastic impedance have limited lithology discrimination capability in sequence 1 due to the presence of organic

rich shale and less density contrast

P-impedance of hydrocarbon sand and wet sand falls in the same ranges but in far-angle elastic impedance, hydrocarbon sand shows relatively lower values than wet sand. Furthermore, crossplots between far-angle and near-angle elastic impedance can delineate the potential hydrocarbon bearing zone

7. Acknowledgements

I would like to express my appreciation to my thesis supervisor Professor Angus John Ferguson for his patient support, guidance, and encouragement of this research work. I also express my deep gratitude to Professor Naseer Ahmad for his enthusiastic advice, and encouragement. I would like to thank Professor Joseph Lambiase, and Professor John Warren for their knowledge through the Petroleum Geoscience Program.

8. References

Connolly, P., 1999. Elastic impedance: The Leading Edge, v. 18, p. 438-452.

Dangprasitthiporn, M., 2015, Lithology prediction using rock physics and acoustic impedance for reservoir distribution in northern of the Pattani Basin, Gulf of Thailand: M.Sc. thesis, Chulalongkorn University, 40 p.

Jardine, E., 1997, Dual Petroleum Systems Governing The Prolific Pattani Basin Offshore Thailand: Proceedings of the Petroleum Systems of SE Asia and Australasia Conference, May 1997, p. 351-363.

Kachi, T., Yamada, H., Yasuhara, K., et al., 2005, Fault-seal analysis applied to the Erawan gas-condensate field in the Gulf of Thailand: AAPG Memoir 85, p. 59 – 78.

Li, Y., Guo, Z., Liu, C., et al., 2015, A rock physics model for the characterization of organic-rich shale from elastic properties, Petroleum Science, v. 12, issue 2, p.264-272.

Marion, D., 1990, Acoustical, mechanical, and transport properties of sediments and granular materials, Ph.D. thesis, Stanford University, 136p.

Morley, C.K., and Racey, A., 2011, Tertiary stratigraphy, in M.F. Ridd, A.J. Barber, and M.J. Crow, eds., The geology of Thailand: Geological Society of London, p. 223-271.

Narapan, J., 2015, Different types of organic-rich geological markers in south Pailin Field, Pattani Basin, Gulf of Thailand: M.Sc. thesis, Chulalongkorn University, 51 p.

Rigo de Righi, L., Baranowski J., Chaikiturajai C., Nelson G., Wechsler D., and Mattingly G., 2003, Block B8/32, Gulf of Thailand: Petroleum System and Implementation of Technology in Field Development: SEAPEX Press, v.6, issue 5, p.46-58.

Veeken, P. C. H., and Da Silva, M., 2004, Seismic inversion methods and some of their constraints, first break, v. 22, p. 47-70.